14th European Signal Processing Conference (EUSIPCO 2006), Florence, Italy, September 4-8, 2006, copyright by EURASIP

MODEL-BASED ROBUST VARIATIONAL METHOD FOR MOTION DE-BLURRING

Takahiro Saito, Taishi Sano, and Takashi Komatsu

Dept. of Electronics and Informatics Frontiers, High-Tech Research Center, Kanagawa University
3-27-1 Rokkakubashi, 221-8686, Yokohama, Japan
phone: +(81)45 481 5661, fax: +(81)45 491 7915, email: {saitot01, R200570084, komatt01}@kanagawa-u.ac.jp
web: www.ku-hrc.jp

ABSTRACT

Once image motion is accurately estimated, we can utilize those motion estimates for image sharpening and we can remove motion blurs. First, this paper presents a variational motion de-blurring method using a spatially variant model of motion blurs. The standard variational method is not proper for the motion de-blurring, because it is sensitive to model errors, and occurrence of errors are inevitable in motion estimation. To improve the robustness against the model errors, we employ a nonlinear robust estimation function for measuring energy to be minimized. Secondly, we experimentally compare the variational method with our previously presented PDE-based method that does not need any accurate blur model.

1. INTRODUCTION

Relative motion between the objects in a scene and the camera during the aperture time gives rise to spatial blurring, which is referred to as the motion blur [1]. The motion blur can be modeled approximately by a 1-D spatial integration. In a moving image sequence, each pixel undergoes the 1-D spatial integration along the direction of its local image motion, and the resultant motion blur is linear but shift-variant. Once local image motion is accurately estimated for every pixel of a given input image sequence, we can utilize those motion estimates for sharpening the image sequence and thus we can remove motion blurs selectively. Since motion blur is spatially variant, a simple linear pseudo-inverse filtering technique is not applicable. To remove motion blurs, a spatially variant model of motion blurs should be taken into account.

This paper presents a variational motion de-blurring method minimizing the regularized energy functional that is defined with a spatially variant model of motion blurs. Since the method adopts the spatially variant model, unlike the usual case of spatially invariant image blur, the minimization problem cannot be solved in a closed straightforward way, and it leads to an iterative sharpening algorithm. The standard regularized variational method uses a square function to measure energy of a solution function [2]~[3], and it employs the energy functional composed of both the data-fidelity energy term to measure energy of a deviation of an input noisy blurred image from the assumed model of motion blurring and the regularization energy term to impose smoothness constraints on a solution function. However, the standard regularized variational method is not necessarily proper for the problem of motion de-blurring, because it is sensitive to model errors [2]~[3], and the occurrence of errors are inevitable in local motion estimation, to make matters worse. To improve the robustness of the variational motion de-blurring method against model errors, we introduce a robust estimation function [4] into the data-fidelity energy term. Furthermore, we experimentally compare the variational method with our previously presented PDE-based method [5]~[6] that does not need any accurate model of motion blurs, particularly from the point of robustness against model errors caused by erroneous motion estimation.

2. MODEL-BASED VARIATIONAL METHOD FOR MOTION DE-BLURRING

2.1 Spatially variant model of motion blurs

First we formulate the model of motion blurs as the linear degradation model at each pixel P(x, y) on the 2D image plane Ω defined as a subset in $\mathbf{R}^2$. Let I (x, y) be an input degraded image containing motion blurs. The input image I (x, y) is defined on the 2D image plane Ω. Then the model of the motion blurs is formulated as the operation:

$$I(x,y) = \varphi \circ f(x,y) + w(x,y) \quad , \tag{1}$$

where f (x, y) is an original image, w (x, y) is independently and identically distributed (IID) additive noise, and φ is a motion-blurring operator. The motion-blurring operator φ is defined as the 1-D integration of original intensity along a motion vector $\mathbf{V}(x,y)=(Vx(x,y),\ Vy(x,y))^T$ at each pixel P(x, y). Hence the motion-blurring operator φ is linear, but not spatially invariant, and it cannot be expressed as an operation of the simple spatial convolution. The effect of the motion blurring is formulated as the spatially variant integral transformation:

$$\begin{aligned} I(x,y) &= \varphi \circ f(x,y) + w(x,y) \\ &= \iint_{\Phi} \eta(x',y';x,y) \cdot f(x+x', y+y') \cdot dx' \cdot dy' + w(x,y), \end{aligned} \tag{2}$$

$\eta(x',y';x,y)$: Kernel function at a pixel $\mathrm{P}(x,y)$

Φ : Range of variables (x',y') of $\eta(x',y';x,y)$

where the kernel function η (x', y'; x, y) is dependent on a motion vector at a pixel P(x, y). In the following, assuming that the temporal integration of incident light during an aperture time between t-1/2 and t+1/2 yields pixel intensity of a frame at time t, we define the kernel function η (x', y'; x, y). Discretizing the integral transformation of (2) and reformulating it as a spatially variant weighted sum, we get the discrete form:

$$I_{i,j} = [\varphi \circ f]_{(i,j)} + w_{i,j} = \sum_{(k,l)\in\Phi} \eta_{k,j;\,i,j} \cdot f_{i+k,j+l} + w_{i,j} \ , \tag{3}$$

$I_{i,j}$, $f_{i,j}$, $w_{i,j}$: Values of I, f, w at a pixel $\mathrm{P(x,y)}$

$\eta_{k,j;\,i,j}$: Discrete weight pattern at a pixel $\mathrm{P(x,y)}$

Φ : Range of indices of the discrete weight pattern $\eta_{k,j;\,i,j}$

$$\Phi = [\,-M, -M+1, \cdots, -1, 0, 1, \cdots, M-1, M\,]^2$$

where $\eta_{k,l;\,i,j}$ is a $(2M+1)\times(2M+1)$ discrete weight pattern characterizing an operation of a weighted average along a motion

vector $\mathbf{V}_{i,j}$ at each pixel P(i, j). The discrete weight pattern is approximately estimated by taking a spatial aperture of each pixel into account. In this paper, assuming that each pixel has a spatial aperture of a circle with a diameter of a pixel interval, in advance we form the discrete weight patterns η for various motion vectors $\mathbf{V}=(Vx, Vy)^T$ whose components are given by pixel accuracy and use the patterns for $\eta_{k,l;i,j}$ in (3).

2.2 Iterative variational sharpening algorithm

A pseudo-inverse operation of the motion-blurring operator φ restores an image by minimizing the data-fidelity energy to measure a deviation of a solution function from the assumed model of motion blurs, but it is generally unstable [7], and the motion de-blurring problem is a typical ill-posed problem. To convert an ill-posed problem to a well-posed one, the regularization of the solution function f is applied. For that purpose, first we employ the energy functional composed of the data-fidelity energy term and the regularization energy term, as follows:

$$E[f]=\iint_{\Omega}\left[\rho_r\left(\|\nabla f\|\right)+\lambda\cdot\rho_d\left(\varphi\circ f-I\right)\right]\cdot dx\cdot dy\,, \tag{4}$$

$\rho_r(z)$, $\rho_d(z)$: Energy cost functions of a variable z

where the functions ρ_r, ρ_d are energy cost functions. The first term in the energy functional $E[f]$ is the regularization energy term, and it imposes smoothness constraints on the solution function f defined on the image plane Ω. If we employ a square function $z^2/2$ as the cost function $\rho_r(z)$, it will produce an over-smoothing effect on the solution function f. Hence, a robust M-estimation cost function [4] is preferable, and it suppresses a smoothing effect in image regions whose intensity gradients are very high. On the other hand, the second term in the energy functional $E[f]$ is the data-fidelity energy term, and it restrains the solution function f from drifting away from the model of motion blurs of (1). For this data-fidelity energy term, also, a robust M-estimation cost function is preferable, because motion estimation is not necessarily reliable, and inevitable errors in motion estimation will produce severe artifacts on the solution function f, in the case of adopting the square cost function $z^2/2$. To suppress a bad influence of a large data-fidelity error $z=\varphi\circ f-I$ produced by poor motion estimation, a robust M-estimation cost function should be adopted. The parameter λ in the energy functional $E[f]$ of (4) controls the balance of the influence of the two energy terms. If λ is too large, the minimization of $E[f]$ will be unstable and very sensitive to random noise, and it will reduce to the pseudo-inverse de-blurring as λ goes to infinity. Conversely, if λ is too small, the regularization energy term have an unnecessary over-smoothing effect on the solution function f. In this paper, taking into account particularly the robustness against random noise, the value of the parameter λ is experimentally determined, and in addition the two nonlinear functions ρ_r, ρ_d are selected through experiments. As the functions ρ_r, ρ_d, the combination of the following two functions achieves well-balanced de-blurring with fidelity and stability.

$$\rho_r(z)=\frac{K_r^{\,2}}{2}\cdot\log_e\left(1+\left(z/K_r\right)^2\right)\ :\text{Cauchy function}\,, \tag{5}$$

$$\rho_d(z)=\begin{cases}\dfrac{K_d^{\,2}}{6}\cdot\left\{1-\left(1-\left(z/K_d\right)^2\right)^3\right\}\,, & |z|\le K_d\\ K_d^{\,2}/6\,, & |z|>K_d\end{cases} \tag{6}$$

: Bi-weight function .

The use of the Cauchy function in the regularization energy term produces a selectively smoothing effect of the Perona-Malik nonlinear diffusion type [8] on the solution image function f. The bi-weight function behaves approximately as the square cost function $z^2/2$, when the magnitude of a data-fidelity error $z=\varphi\circ f-I$ is small; it replaces z by a constant value $K_d^{\,2}/6$ when the magnitude of a data-fidelity error $z=\varphi\circ f-I$ exceeds a threshold value K_d. The optimal values of the parameters K_r, K_d characterizing the two functions ρ_r, ρ_d are dependent on variance of additive random noise and tolerance to model errors, respectively. In this paper, the parameter K_r is fixed at 5, whereas the parameter K_d is fixed at 30. These parameter values are selected empirically. For comparison, this paper experimentally studies the model-based PDE method that uses the square function $z^2/2$ for energy cost function ρ_d.

The Euler-Lagrange equation minimizing the energy functional $E[f]$ of (4) is given by the nonlinear PDE:

$$\lambda\cdot\varphi^*\circ\psi_d\left(\varphi\circ f-I\right)-div\left[\psi_r\left(\|\nabla f\|\right)\cdot\nabla f\right]=0\,, \tag{7}$$

$$\psi_r(z)=\frac{1}{z}\cdot\frac{d}{dz}\rho_r(z)=\frac{1}{1+\left(z/K_r\right)^2}$$

$$\psi_d(z)=\frac{d}{dz}\rho_d(z)=\begin{cases}z\cdot\left(1-\left(\dfrac{z}{K_d}\right)^2\right)^2\,, & if\quad |z|\le K_d\\ 0\,, & if\quad |z|>K_d\end{cases}$$

where the Neumann boundary condition is applied. The second term in the nonlinear PDE of (7) is the nonlinear diffusion term, and the function $\psi_r(z)$ is a nonlinear function determining its nonlinear diffusion coefficient. On the other hand, the function $\psi_d(z)$ in the first term is the robust influence function that is defined as the first order derivative of the bi-weight function of (6); if the magnitude of a data-fidelity error $z=\varphi\circ f-I$ exceeds the threshold value K_d, the influence of the data-fidelity error will be set at zero and will be neglected The operator φ^* in the first term is an adjoint operator of the motion-blurring operator φ, and it is defined by the integral transformation:

$$\varphi^*\circ z(x,y)=\iint_{\Phi}\left\{\eta\left(x'',y'';x-x'',y-y''\right)\cdot z\left(x-x'',y-y''\right)\right\}dx''\,dy''\,. \tag{8}$$

The discrete form of the adjoint operator φ^* is expresses as

$$\left[\varphi^*\circ f\right]_{(m,n)}=\sum_{(i,j)\in\Omega}\eta_{m-i,n-j;i,j}\cdot f_{i,j}=\sum_{(k,l)\in\Phi}\eta_{k,l;m-k,n-l}\cdot f_{m-k,n-l} \tag{9}$$

Ω : Support of the image function f

Φ : Range of indices (k,l) of the discrete weight pattern $\eta_{k,j;i,j}$

$$\Phi=\left[-M,-M+1,\cdots,-1,0,1,\cdots,M-1,M\right]^2$$

where the subset Ω is the support of the solution image function f and the subset Φ is the range of indices (k, l) of the discrete weight pattern $\eta_{k,l;i,j}$ of the operator φ. Since the adjoint operator φ^* as well as the motion-blurring operator φ is linear, but spatially variant, the Discrete Fourier Transform technique [7] is not utilized to solve the PDE of (7) in a non-iterative way. Its solution requires an iterative method.

Starting from the Euler-Lagrange PDE of (7), we derive a discrete iterative sharpening algorithm as follows. Introducing an artificial time variable τ and replacing the image function $f(x, y)$ by the time-evolving image function $f(x, y;\tau)$, we reformulate (7) as the time-evolution PDE of the image function $f(x, y;\tau)$:

$$\partial_\tau f=div\left[\psi_r\left(\|\nabla f\|\right)\cdot\nabla f\right]-\lambda\cdot\varphi^*\circ\psi_d\left(\varphi\circ f-I\right). \tag{10}$$

$$\text{Initial condition:}\quad f(x,y;0)=I(x,y)$$

where ∂_τ is the first-order partial derivative operator with respect to the artificial time variable τ. Initializing the time-evolving image function $f(x, y; \tau)$ as the input motion-blurred image $I(x,y)$ and then evolving the image function $f(x, y; \tau)$ according to (10), the image function $f(x, y; \tau)$ will converge to the solution image function of the Euler-Lagrange PDE of (7). Thus the steady-state solution of the time-evolution PDE of (10) is employed as a sharpened recovery image. The actual discrete iterative sharpening algorithm is derived by discretizing the time-evolution equation of (10). In the discretization, the forward-difference approximation is applied to the partial derivative operator ∂_τ, the standard Perona-and-Malik discretization technique [8] is applied to the calculus of the nonlinear diffusion term, and equations of (3) and (9) are used for the computation of the motion-blurring operator φ and its adjoint operator φ^*.

The discrete iterative sharpening algorithm is as follows:

$$\begin{cases} z_{m,n}^{(\tau)} = \left(\sum_{k=-M}^{M} \sum_{l=-M}^{M} \eta_{k,l;m,n} \cdot f_{m+k,n+l}^{(\tau)} \right) - I_{m,n} \\ f_{m,n}^{(\tau+1)} = f_{m,n}^{(\tau)} + \varepsilon \cdot \left[\sum_{D=N,S,E,W} \left\{ \psi_r \left(\left| \nabla_D f_{m,n}^{(\tau)} \right| \right) \cdot \nabla_D f_{m,n}^{(\tau)} \right\} \right. \\ \qquad \left. - \lambda \cdot \left\{ \sum_{\tilde{k}=-M}^{M} \sum_{\tilde{l}=-M}^{M} \eta_{\tilde{k},\tilde{l};m-\tilde{k},n-\tilde{l}} \cdot \psi_d \left(z_{m-\tilde{k},n-\tilde{l}}^{(\tau)} \right) \right\} \right] \end{cases} \tag{11}$$

$$\nabla_N f_{m,n}^{(\tau)} = f_{m,n-1}^{(\tau)} - f_{m,n}^{(\tau)}, \quad \nabla_S f_{m,n}^{(\tau)} = f_{m,n+1}^{(\tau)} - f_{m,n}^{(\tau)}$$

$$\nabla_E f_{m,n}^{(\tau)} = f_{m+1,n}^{(\tau)} - f_{m,n}^{(\tau)}, \quad \nabla_W f_{m,n}^{(\tau)} = f_{m-1,n}^{(\tau)} - f_{m,n}^{(\tau)}$$

$f_{m,n}^{(\tau)}, z_{m,n}^{(\tau)}$: values of f, z on the pixel location $\mathrm{P}(m,n)$ at the τ-th iteration

Initialization : $f_{m,n}^{(0)} = I_{m,n}$

In (11), for a stationary pixel whose motion vector is a zero vector, as the motion-blurring operator φ we set the identity operator ϑ that for an arbitrary image function satisfies the property $\vartheta \circ f = f$. The intermediate variable $z^{(\tau)}$ in (11) is a deviation of the computed motion-blurred image $\varphi \circ f^{(\tau)}$ from the actual motion-blurred image I, and the adjoint operator φ^* is applied to the deviation $z^{(\tau)}$. The parameter ε is a parameter to control the speed of iterations. At each iteration cycle, first the deviation $z^{(\tau)}$ is computed, and then the time-evolving image function $f(x, y; \tau)$ is updated. The iteration cycle is repeated until convergence. Actually, when the relative magnitude of updates for the entire time-evolving image function $f(x, y; \tau)$ at the τ-th iteration is under a small threshold value, the iteration cycle is automatically stopped.

In addition to the de-blurring method of (10), for comparison, we experimentally study a kind of pseudo-inverse model-based de-blurring method that minimizes the data-fidelity energy defined with the energy cost function ρ_d that is either the Cauchy function or the square function $z^2/2$, and its basic time-evolution equation is given by

$$\partial_\tau f = -\varphi^* \circ \psi_d (\varphi \circ f - I). \tag{12}$$

$$\text{Initial condition} : f(x, y; 0) = I(x, y)$$

3. EVALUATION OF SHARPENING PERFORMANCE

In this paper, to evaluate sharpening performance of the motion de-blurring methods separately from motion estimation, we assume that true motion vectors are given, and without estimating motion vectors we perform experimental simulations of the motion de-blurring. For the quantitative performance evaluation, we use a test moving image sequence containing artificial motion blurs, and we compute the peak SN ratio *PSNR* [dB] between the sharpened image and the original sharp image. First, we synthesize a motion-blurred test image sequence on the assumption that in front of a stationary background image a smaller sharp image plane moves with a constant velocity $\mathbf{V}=(V_x, V_y)^T$, and then we add random Gaussian noise with zero mean and standard deviation of 3.0, to the blurred image sequence; thus we generate a test moving image sequence. Fig.1(a) shows the original small sharp image embedded in the original background image, and Fig.1(b) shows the motion-blurred test image generated by fixing the motion vector $\mathbf{V}$ of the embedded small image at $(3,3)^T$. In Fig.1(b), motion blurs appear along the direction of the motion vector $(3,3)^T$. In the simulations, we set the vector of $(3,3)^T$ as the true motion vectors at all pixels in the embedded moving small image, whereas we set the vector of $(0,0)^T$ as the true motion vectors at all pixels in the stationary background image region outside the embedded moving small image; the true motion vectors are used for constructing the motion-blurring operator φ. In addition, we fix the parameters { ε, λ, K_r, K_d } at { 0.05, 1.0, 5.0, 30 } respectively, and these values are determined through experiments.

For comparison we experimentally study the five different motion de-blurring methods:

(a) Model-based motion de-blurring method A that employs the bi-weight function of (6) as the energy cost function ρ_d in the time-evolution PDE of (10),

(b) Model-based motion de-blurring method B that employs the square function as the energy cost function ρ_d in the time-evolution PDE of (10),

(c) Model-based motion de-blurring method C that employs the bi-weight function of (6) as the energy cost function ρ_d in the time-evolution PDE of (12),

(d) Model-based motion de-blurring method D that employs the square function as the energy cost function ρ_d in the time-evolution PDE of (12),

(e) Model-free motion de-blurring method E Previously we presented a model-free PDE method that does not need any accurate model of motion blurs [5], [6]. This model-free PDE method is based on a coupled nonlinear diffusion process that is composed of a nonlinear diffusion term, an anisotropic peaking term and a fidelity term. Since motion blurs are anisotropic, as the peaking term we employed the anisotropic peaking term that produces overshoots steered in direction of motion at each pixel. Unlike the model-based method, the model-free method uses a transient image of the time-evolution

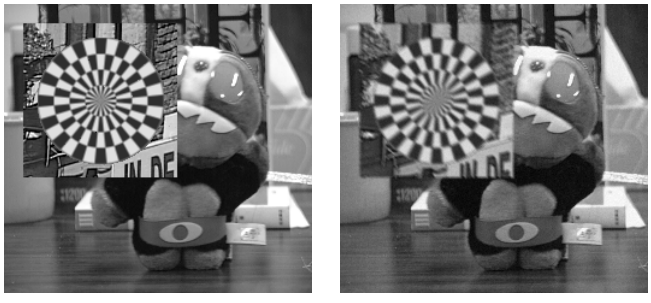

(a) Original small sharp image embedded in the original background image

(b) Motion-blurred test image generated by fixing the motion vector $\mathbf{V}$ of the embedded small image at $(3,3)^T$

Figure 1 - Original image and the motion-blurred test image

PDE as a sharpened image. Our proposed decision scheme to stop the time-evolution halts the iteration almost at the ideal moment when the time-evolution achieves the best selective sharpening.

Under the ideal condition that the true motion vectors are given, we apply the five different motion de-blurring methods to the motion-blurred test image of Fig.1(b), and compute an improvement in the peak SN ratio *PSNR* [dB] of each sharpened image over the motion-blurred test image. Table 1 compares the *PSNR* improvements for the five different motion de-blurring methods, and it shows both the *PSNR* improvements within the embedded moving small image and those over the whole image. Fig.2 compares the sharpened images given by the three different motion de-blurring methods A, C.

In table 1, the model-based motion de-blurring methods A, B, C, D give higher *PSNR* improvements than the model-free motion de-blurring method E. In the ideal case that the true motion vectors are given, the comparison between the method A and the method B, or between the method C and the method D, shows that the model-based method using the square function provides a somewhat higher *PSNR* improvement than the model-based method using the bi-weight function. If the true motion vectors are given, the square function will be preferable to robust *M*-estimation cost functions. As shown in Fig.2, the model-based method C, which are not reinforced with the regularization, produces noticeable artificial checked pattern in the image region of the embedded small moving image; whereas the model-based method A, which are armed with the regularization, does not produce such artifacts and provides a subjectively good quality sharpened image. On the other hand, the model-free method E excessively flattens original small intensity variations, and its sharpened image gives a visually artificial impression [5], [6]; whereas the model-based method A reproduces edges and textures more clearly, and the visual impression of its sharpened image is more vivid.

Moreover, to evaluate the robustness of the motion de-blurring methods against errors in the model of motion blurs, we add statistically independent Gaussian noise with zero mean and standard deviation σ_v to each component of the true motion vector at each pixel, and then omit its decimals; we use the resultant noisy motion vectors for constructing the motion-blurring operator φ at each pixel. Fig.3 compares the sharpened images given by the two different motion de-blurring methods A, B in the case of σ_v=1.25, where for approximately two thirds of all the pixels their motion vectors do not coincide with the true motion vectors. Fig.4 compares the update characteristics of the motion de-blurring methods A, B for various values of the standard deviation σ_v, and it shows both the update characteristics within the embedded moving small image and those over the whole image.

The model-free motion de-blurring method E, which does not utilize the model of motion blurs and uses only the direction of image motion, is very robust against errors in motion estimation. Even if artificial errors are added to the true motion vectors, the model-free motion de-blurring method E provides a sharpened image that is in no way visually inferior to that provided under the ideal condition that the true motion vectors are given. On the other hand,

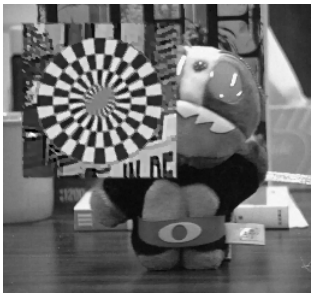

(a) Motion de-blurring method A

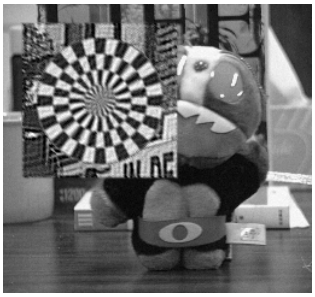

(b) Motion de-blurring method C

Figure 2 - Sharpened images when the true motion vectors are given at all pixels

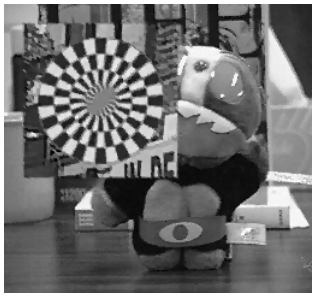

(a) Motion de-blurring method A

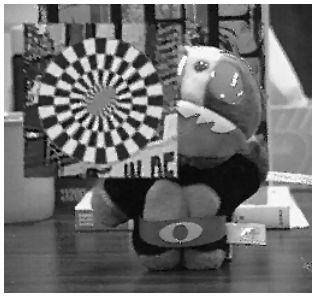

(b) Motion de-blurring method B

Figure 3 - Sharpened images when independent Gaussian noise with zero mean and standard deviation σ_v of 1.25 is added to each component of the true motion vectors at all pixels

Table 1 - Comparison of the sharpening performance of the model-based motion de-blurring methods and the model-free motion de-blurring method in the model-error-free case: improvement in *PSNR* [dB] of the sharpened image over the motion-blurred test image

Motion de-blurring method				*PSNR* improvement [dB]	
Abbr.	Model-based / Model-free	Time-evolution PDE	Energy cost function for the data-fidelity energy term	Within the embedded moving small image	Over the whole image
A	Model-based	Equation 10	Bi-weight function	2.30 [dB]	1.94 [dB]
B	Model-based	Equation 10	Square function	2.58 [dB]	2.17 [dB]
C	Model-based	Equation 12	Bi-weight function	2.33 [dB]	1.99 [dB]
D	Model-based	Equation 12	Square function	2.43 [dB]	2.07 [dB]
E	Model-free	Ref. [5] & [6]	None	1.94 [dB]	1.50 [dB]
PSNR [dB] of the motion-blurred test image				19.43 [dB]	24.63 [dB]

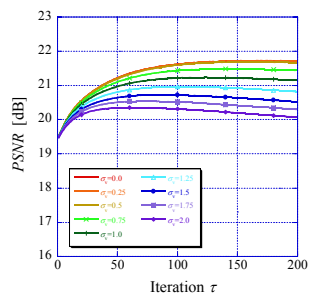

(a) Update characteristics of the motion de-blurring method A within the embedded moving small image

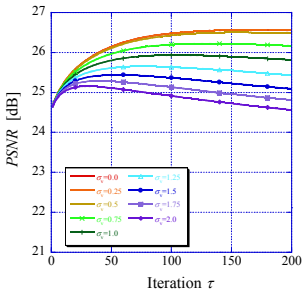

(b) Update characteristics of the motion de-blurring method A over the whole image

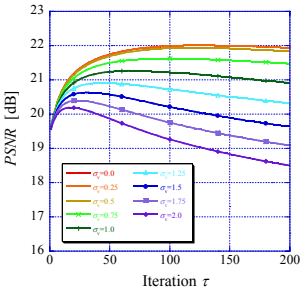

(c) Update characteristics of the motion de-blurring method B within the embedded moving small image

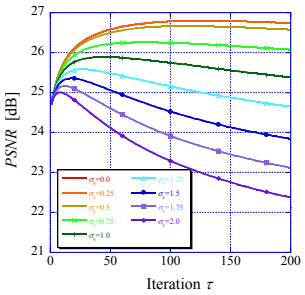

(d) Update characteristics of the motion de-blurring method B over the whole image

Figure 4 - Update characteristics of the motion de-blurring methods A, B when independent Gaussian noise with zero mean and standard deviation σ_v is added to each component of the true motion vectors at all pixels

the model-based motion de-blurring methods A, B, which utilize the steady-state solution of the time-evolution PDE as a sharpened image, will produce a steady-state solution containing visible artifacts if the standard deviation σ_v is rendered a large value. The model-based motion de-blurring method B employs the square function as the energy cost function ρ_d, and its update characteristics will considerably degrade if the standard deviation σ_v exceeds 1.0, where for approximately half pixels their motion vectors do not coincide with the true motion vectors. On the other hand, in the model-based motion de-blurring method A, which employs the bi-weight function as the energy cost function ρ_d, the deterioration of its update characteristics is fairly alleviated. When the standard deviation σ_v is fixed at 1.0, within the embedded moving small image the model-based motion de-blurring method A gives the *PSNR* improvement of about 1.7 [dB] over that of the motion-blurred test image; over the whole image its update characteristics somewhat degrade, but the peak SN ratio *PSNR* [dB] of its sharpened image is improved by about 1.2 [dB] over that of the motion-blurred test image.

As shown in Fig.3(b), the model-based motion de-blurring method B sharpens motion blurs, but produces visible spot artifacts. On the other hand, the model-based motion de-blurring method A suppresses the occurrence of the visible spot artifacts considerably, as shown in Fig.3(a). In Fig.3(b), such spot artifacts appears clearly not only in the embedded moving small image region, but also in the image region of the stationary background. Those spot artifacts get the deterioration of the update characteristics over the whole image more severer than within the embedded moving small image. In the image region of the stationary background, as the motion-blurring operator φ some operator other than the identity operator ϑ is used, and unnecessary sharpening is performed; thus the visible spot artifacts are generated. On the other hand, even if the moving image region is judged to be still by mistake, no artifacts will be produced, because the identity operator ϑ is employed as the motion-blurring operator φ and hence no image sharpening will be performed. Therefore, in practical applications of the model-based motion de-blurring method A, in advance of the motion de-blurring, stationary image regions, where the identity operator ϑ is employed as the motion-blurring operator φ, should be detected reliably.

4. CONCLUSIONS

For the motion de-blurring, this paper presents a model-based PDE method minimizing the energy functional that is defined with a spatially variant model of motion blurs. To enhance the robustness of the model-based PDE method against model errors, we adopt robust estimation functions for measuring energy to be minimized. Moreover, this paper experimentally compares the model-based PDE method with our previously presented model-free PDE method that does not need any accurate blur model, from the point of robustness against model errors caused by erroneous motion estimation. Experimental simulations demonstrated that in the model-error-free case the model-based PDE method outperforms the model-free PDE method, but in the model-error case the latter works better than the former. In the model-error case, to alleviate the deterioration of the sharpening performance, in advance of the application of the model-based PDE method, stationary image regions should be detected reliably. At present, we are studying the application of our motion de-blurring methods to real image sequences taken with a digital movie camera.

REFERENCES

[1] A. Rosenfeld and A.C. Kak: Digital picture processing, Ch.6.4.2., *Academic Press, Inc.*, New York, 1982.

[2] G. Aubert and P. Kornprobst: Mathematical problems in image processing – Partial differential equations and the calculus of variations, *Springer Verlag*, New York, 2002.

[3] G. Auber and L. Vese: A variational method in image recovery, *SIAM J. Num. Anal.*, **34**, 5, pp.1948-1979, 1997.

[4] A. B. Hamza, H. Krim and G. B. Unal: Unifying probabilistic and variational estimation, *IEEE Signal Process. Mag.*, **19**, 5, pp.37-47, 2002.

[5] T. Saito, H. Harada and T. Komatsu: Motion de-blurring by coupled nonlinear diffusion using an anisotropic peaking term, *Proc. Visualization, Imaging, and Image Processing*, pp. 796-801, 2004.

[6] T. Saito, H. Harada and T. Komatsu: Extension of coupled nonlinear diffusion to motion de-blurring: introduction of anisotripic peaking: *J. Institute of Image Information & Television Engineers*, **58**, 12, pp.1839-1844, 2004.

[7] M. R. Banham and A.K. Katsaggelos: Digital image restoration, *IEEE Signal Process.* Mag., **14**, 2, pp.24-41, 1997.

[8] P. Perona and J. Malik: Scale-space and edge detection using anisotropic diffusion: *IEEE Trans. Pattern. Anal. & Mach. Intell.*, **12**, 7, pp.629-639, 1990.